Design and Characterization of a Test Bench For Interior Noise Investigations

Ling Liu, Francesco Ripamonti and Roberto Corradi

Department of Mechanical Engineering, Politecnico di Milano, Milano 20156, Italy.

Zhushi Rao

State Key Laboratory of Mechanical System and Vibration, School of Mechanical Engineering, Shanghai Jiao Tong University, Shanghai 200240, China. E-mail: zsrao@sjtu.edu.cn

(Received 9 February 2022; accepted 15 June 2022)

The increasing demand for acoustic comfort in vehicles has popularized the vibroacoustic analysis using computer-aided engineering (CAE) tools and boosted the development of various noise control measures. Concerning the often-unknown reliability of a CAE tool and the high cost of testing control strategies in a real vehicle, this paper proposes a test bench called Noise-Box, for benchmarking the CAE tools and testing new control measures. The test bench is designed towards a simple plate-cavity system that is easy to model and analyze, so that any vibroacoustic test performed on it can be accurately reproduced by numerical models. Specifically, it is a concrete box with six rigid walls and an opening that can be covered by flexible or soundproofing panels. The complete design is elaborated, including the cavity's shape and dimensions, the panel's installation and the device's overall configuration. Moreover, the acoustic field provided by the test bench is characterized for the typical features that will guide the device's future applications, covering modal property, reverberation time (or sound absorption) and field diffuseness. This work could be informative and instructive not only for the presentation of the novel test bench but also for the utilized methodologies in its design and characterization.

1. INTRODUCTION

Recently, people are paying more and more attention to the acoustic comfort of their vehicles, as well as the health issues caused by noise. For various types of vehicles (e.g., automobiles, trains, aircrafts, etc.) requests are being made for a better acoustic design. Many efforts have helped with the reduction of interior noise,[1–7] but it is still a challenging task, especially when the vehicles are now under the trend towards lightweight design and toward new energy replacement.[8,9]

In developing the techniques to mitigate/control noise, it is important for the manufacturers that the techniques themselves as well as the developing processes are cost effective.[10] Fortunately, the recently rapidly-developing computer-aided engineering (CAE) tools significantly save costs in the design stage. The CAE tools are able to simulate the dynamic and acoustic behaviors of a product with virtual prototypes, where modifications are easy to apply and the added costs are considerably lower than the traditional physical prototypes. However, this advantage relies on the availability and reliability of CAE tools for studying the problem. In terms of availability, the vehicle interior noise is a typical vibroacoustic problem, so CAE tools for the vibroacoustic analysis can be used. Though CAE tools are now widely used in vehicle industries, their capability with respect to the vibroacoustic simulations is limited. One of the limitations is the so-called 'mid-frequency gap'.[11] This issue has been pointed out since the 1990s but still puzzles engineers and researchers. With respect to reliability, it is an important issue whenever we are developing or using a predictive tool. In this regard, the significance of benchmarks for the vibroacoustic software has been noticed in many studies.[12–14] As more and more in-house or commercial tools are developed, common benchmark cases for validation or assessment are scarce. The lack of benchmarks does hamper the development of new predicting techniques, hinder the improvement of existing numerical methods and waste the time and effort of researchers and engineers. However, in the development of new methods and new codes for vibroacoustic analysis for over 30 years, a well-known and authorized benchmark database has not yet been established, though the outcomes of some attempts are trackable online.[15–17] For example, NASA had 4 workshops which studied benchmark problems of aeroacoustics in 1995-2003. The numerical solutions worked out by researchers were finally presented as proceedings.[15] A benchmark platform was last updated in 2015, and was established by researchers from Japan, Korea and Malaysia. This benchmark platform focused on the computational methods for architectural or environmental acoustic.[16] Around 2015, a more recent platform was built by the European Acoustics Association (EAA) for benchmark cases in computational acoustics.[14,17] These attempts provide some benchmark cases, but few of them are associated with vehicle interior noise issues or possess experimental results as a reference. In fact, as a benchmark, the experimental results should come from a well-characterized test bench. Hence, this work proposes such a test bench called, *Noise-Box,* that can be easily reproduced by the numerical models and can provide benchmarks with reference measurements to facilitate the CAE analysis of interior vibroacoustic problems.

Meanwhile, the test bench should be available for the typical vibroacoustic problems involved in vehicle compartments, like the investigation of structure-borne and airborne noises and the

examination of different noise control techniques. Thus, it can be used to validate or debug a new noise control measure in the lab before the implementation of a more complex system. There are interior acoustic/vibroacoustic test benches in literature, but most of them are designed for a single type of tests. Particularly, Del Rey et al.[18] designed and constructed a small-sized reverberation chamber for the measurement of sound absorption; Vivolo[19] proposed a small cabin for the vibroacoustic characterization of lightweight panels; and Cheer[20] created a car cabin mock-up to examine the active noise control strategies. By comparison, the Noise-Box is intended to be multifunctional, serving as the benchmark of numerical models, the characterization of sound absorbing or proofing materials, and the development of noise control measures.

The Noise-Box has been built and used in the PoliMi Sound and Vibration Laboratory (PSVL) of Politecnico di Milano.[21] This work presents the Noise-Box regarding the design of its complete test system and the characterization of its inner sound field. The design originates from the simplification of a vehicle compartment, and the characterization considers some typical features that will guide its future applications. In addition to the promotion of the novel test bench, it is expected that the presented work will be informative and instructive for the development and identification of similar devices.

Owing to the complexity of vehicle interior noise, simplified systems are always used for a knowledge-oriented investigation. The simplification of a vehicle compartment can be classified into three levels. The first level considers only the simplification of geometry, so the compartment is scaled smaller or reduced to a regular shape, but is still surrounded by flexible thin walls.[22–25] In this case, the vibration not only interacts with the acoustic field but also transmits among panels. Since the connection between components is always hard to characterize, such a system is too complicated to be a benchmark tool. The second level falls into a plate-cavity system.[26–35] The system consists of a rigid box and a flexible panel. Thus, without the influence from other panels, it is easier to determine how the panel structure affects the acoustic field inside the box and reversely, how the cavity influences the panel vibration. The plate-cavity system has been widely used for vibroacoustic analysis. For the plate, its structure and boundary conditions are not limited. It can be as simple as an isotropic thin plate subjected to the clamped or simply-supported boundary conditions,[26–29] or as complex as a laminated plate with elastically restrained or non-uniform boundary conditions.[30,31] For the cavity, it can be regularly or irregularly (e.g., car-like) shaped[32,33] with different wall impedance.[34,35] The third level of simplification considers no flexible structure but only the acoustic cavity inside.[36–38] Such a model isolates the cavity from the structure vibration and helps to determine its acoustic properties affected by geometry and wall impedance. This is preferred when the coupling effect between walls and cavity is negligible, and acceptable when the coupling effect is weak or not of interest. However, since the required simplified system is for vibroacoustic analysis where the structure cannot be absent, this simplification is not adopted. Finally, the second level of simplification, i.e., a plate-cavity system is selected for designing the Noise-Box. In addition, when the flexible panel of the plate-cavity system is replaced by a thick rigid wall, the system reaches the third level of simplification and can be used for acoustic field investigation. This arrangement is adopted in this work for the characterization of the Noise-Box's cavity.

Regarding the characterization of the sound field inside an enclosure, some features are generally important for the applications of the room, such as the acoustic modes, the reverberation time or sound absorption and the sound field diffuseness. A good understanding of the modal properties of the enclosed sound field can help to reveal the coupling effects between the panel and the cavity in a plate-cavity system.[39] The reverberation time or sound absorption is crucial for any room with a specific purpose (e.g., concert, conference, acoustic experiment, etc.).[40–43] The sound field diffuseness is also of interest, either for using it as a reverberation room[9,41,44] or for selecting a deterministic or statistic method to model the cavity.[45,46]

Thus, in the following sections, this article first elaborates on the design of the test bench, Noise-Box, and then demonstrates the characterization. In the design section, the set-up principle is introduced at the beginning, pointing out the main considerations. Then, the design methodology and the final design are illustrated, where the cavity shape and dimensions are determined with the intention to maximize the diffuseness within a limited overall size. In the characterization section, the acoustic characteristics of the Noise-Box cavity are identified through experiments and simulations. The experimental set-up and numerical models are first introduced. Then, the cavity modes are obtained, triply validated by the two-dimensional (2D) and three-dimensional (3D) finite element (FE) models and the experimental set-up. The sound absorption is assigned based on the measured reverberation time for 1/3 octave bands. The sound field diffuseness is evaluated using different quantifiers. Among them, the methods and results are illustrated respectively for each characteristic. Finally, conclusions are drawn stressing the methods for designing and characterizing the Noise-Box and the main outcomes.

2. DESIGN OF THE TEST BENCH

2.1. Set-up Principle

The objectives of the test bench are to benchmark the CAE tools for interior vibroacoustic analysis and to test the materials, structures or control strategies for noise mitigation. Hence, the Noise-Box is designed as a plate-cavity system combined with the following considerations:

1. The system should be representative, with access to panel, cavity, structure-borne noise, airborne noise and noise control measures;

2. The system should be easy to model and analyze, with simple geometry and identifiable boundary conditions; and,

3. All geometric, material and physical parameters should be specified.

Due to the numerous possibilities for the shape of the cavity, a passenger car is used as reference here for illustrating the correlation between the plate-cavity system and a vehicle

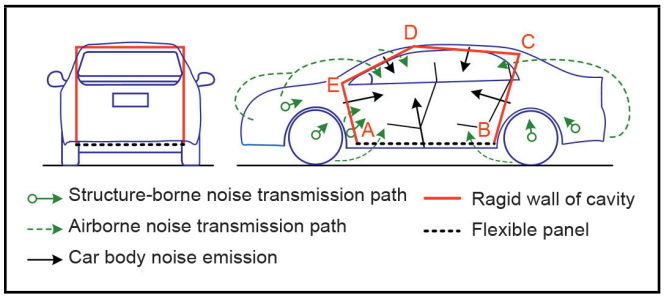

Figure 1. Vehicle interior noise principle and the simplified plate-cavity system

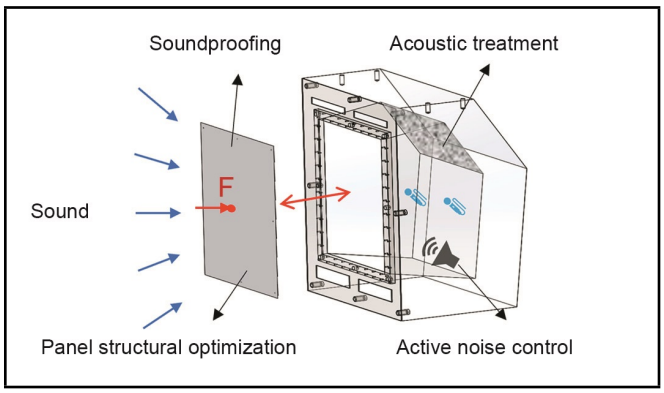

Figure 2. Schematic diagram of the test bench for noise mitigation measures.

compartment, and later for the geometric design of the Noise-Box. The vehicle interior noise considers all noises transmitted into the cabin through the structure-borne or airborne path, as shown in Fig. 1 The plate-cavity system simplifies the car body and the acoustic filed inside. The cavity represents the vehicle compartment, and the panel represents the vibrating car body. When the panel is excited by a mechanical force, the noise inside the cavity is structure-borne and the panel is the only transfer path. When there is a sound excitation outside, the interior noise is airborne and transmitted through the panel. The coupling between structure and enclosed acoustic field is revealed by the coupling between the panel and the cavity.

The plate-cavity simplification makes the test bench more adaptable and multi-functional. On one hand, the system consists of only two components, which is the simplest case for a vibroacoustic system and the best option for benchmarks. It can reveal the structural-acoustic coupling mechanism and validate the numerical methods for interior noise prediction. On the other hand, various noise mitigation measures can be tested in such a test bench. For example, as shown in Fig. 2, optimized panels can be mounted for vibroacoustic tests to validate their performance; soundproofing structures can cover the opening of the cavity to check their sound transmission loss; the wall impedance is changeable with different acoustic treatments; and by placing secondary sound sources inside, the Noise-Box can help to develop active noise control strategies.

2.2. Cavity Design and Optimization

For the determination of cavity shape and dimensions, two criteria are examined:

1. The cavity should be easy to build, model and analyze; and,
2. The acoustic field inside the cavity should be able to represent the acoustic field inside the vehicle compartment.

For the first criterion, simple geometry and physics are preferred, so the walls are shaped flat and built of thick reinforced concrete to approximate the acoustically and mechanically rigid boundary conditions. For the second criterion, it should be noted that the Noise-Box cavity is different from a real compartment of any vehicle. Firstly, the volume is smaller, since the Noise-Box, as a test rig in the lab, should limit its size and weight. Secondly, in accordance with the first criterion, the cavity is geometrically simpler and with fewer diffusers. Hence, the Noise-Box cavity will have a higher first natural frequency, and its sound field diffuseness will not be as good as a real compartment. The design should be optimized for the diffuseness under the constraint of size. The methods used to design small reverberation cabins[19,47,48] are employed for the optimization. In fact, such methods are trying to make the cavity less dominated by a single acoustic mode via the adjustment of mode shapes and natural frequency spacing. Besides, increasing the sound field diffuseness helps the Noise-Box to function as a small reverberation room.

The preliminary shape was originated from the compartment of a passenger car, as shown in Fig. 1. It was simplified into a pentagonal prism, with two side walls parallel to each other and perpendicular to the bottom panel. The bottom flexible panel is rectangularly shaped and larger than other rectangular walls. As the boundary conditions of the flexible panel may be one source of uncertainty to the system, the larger size can make them less significant. The simplification of the two side walls is also reasonable, since many vehicles have symmetric side walls that are close to vertical and the simplification enables the usage of 2D model for the cavity.[1] In numerical simulations, the 2D models are much more efficient than the 3D ones.

With the shape determined, the next step is to settle the ratios of lateral dimensions. In the low frequency region, the modal density is small. One method to improve the diffuseness is to optimize the geometry to achieve a homogeneous distribution of the natural frequencies.[47] For rectangular reverberation rooms, the ratio 1:1.26:1.59 is recommended,[41,49] since it avoids modal degeneracy in a wide frequency range. Although the cavity is not rectangular, the ratio was used as a start point for searching the optimal geometry. In other words, the cuboid that encloses the cavity (shown in Fig. 3) initially satisfies $L_x : L_y : L_z = 1.59 : 1.26 : 1$. Then, the dimensions and shape were adjusted as indicated by the arrows shown in Fig. 3, which indicates modifying the lengths L_x, L_y, L_z and the coordinates of corners A, B, C, D, E. No advanced optimization approach was applied outside of using a simple parametric study with different lengths and coordinates. For each case, the eigenfrequencies and mode shapes of the acoustic field in the low frequency range were computed via finite element method (FEM) and then analyzed in order to seek the best option.

On quantifying the uniformity of the eigenfrequency distribution, the frequency spacing index (ψ) proposed by Bolt[50] was used. This index evaluates the mean square of the deviations of the distances between subsequent modes, which is

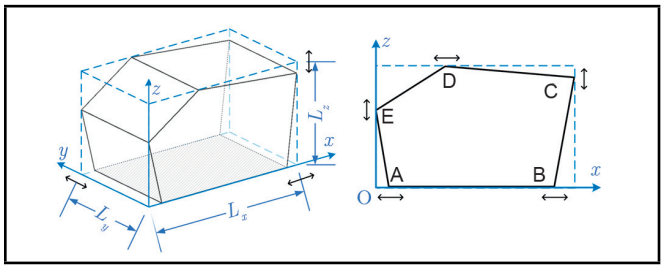

Figure 3. Schematic diagram for optimizing the cavity geometry.

given by:[47,50]

$$\psi = \frac{\sum_{i=1}^{n-1} \varepsilon_i^2}{(n-1)\bar{\delta}^2} + 1; \tag{1}$$

with:

$$\bar{\delta} = \frac{1}{n}\sum_{i}^{n-1} \delta_i = \frac{1}{n}\sum_{i}^{n-1} (f_{i+1} - f_i); \tag{2}$$

$$\varepsilon_i = \left|\delta_i - \bar{\delta}\right|; \tag{3}$$

where n is the total number of modes, δ_i denotes the distance between $(i+1)^{th}$ natural frequency f_{i+1} and i^{th} natural frequency f_{i+1}, $\bar{\delta}$ is the mean value of the distances δ_i, and ϵ_i is the deviation of δ_i from the mean value $\bar{\delta}$.

In Eq. (1), the number n, which determines the upper bound frequency, is also important. One choice of the upper bound frequency is the low-frequency limit of the diffuse field. Blaszak[47] proposed to use the Schroeder frequency:[51]

$$f_s = 2000\sqrt{\frac{T_{60}}{V}}; \tag{4}$$

where T_{60} is the reverberation time and V is the volume of the room. However, since T_{60} is unknown in the design stage and the Schroeder frequency f_s is too restrictive from the application point of view (maybe much higher than the upper bound of modal region), another commonly-used cut-off frequency was adopted. This cut-off frequency corresponds to the modal density of 20 modes per third-octave band and is given by:[44]

$$f_c = \frac{c}{\sqrt[3]{V/4}}; \tag{5}$$

where c denotes the sound speed.

Since a smaller value of ψ means a better uniformity of the eigenfrequency distribution, the optimization is to minimize this value. However, as the index ψ doesn't bring complete information on the non-uniformity,[47] the designer still needs to check the exact eigenfrequency distribution in the process.

2.3. Assembly and Installation

Concerning the assembly and disassembly of the flexible panel to the test bench, a steel frame is mounted to the concrete walls around the opening of the cavity, as shown in Fig. 4(a). The steel mounting frame can mount the panel in two ways: rigidly supported and elastically supported. The two mounting types correspond to two different detail views of the circle area at the point B of Fig. 4(a). Fig. 4(b) shows the detail view for the rigid mounting. A steel clamping frame is placed on the flexible panel and fixed with two circumferential rows of screws to approximate the clamped boundary conditions.

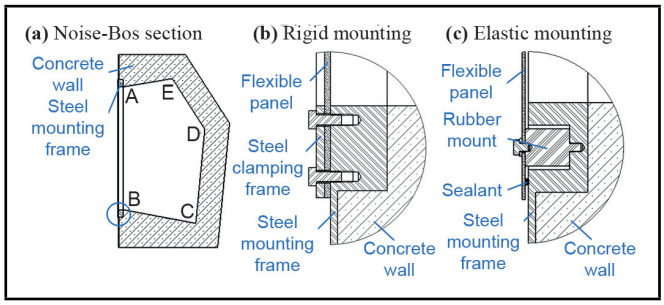

Figure 4. Design for the mounting of flexible panel.

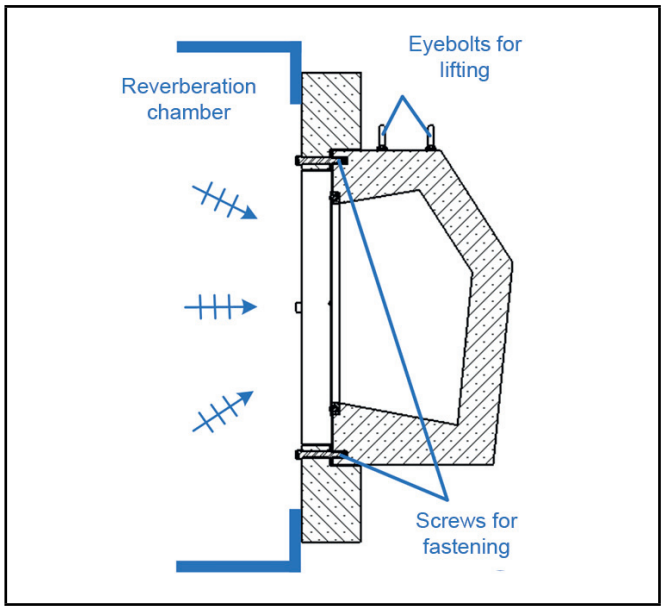

Figure 5. Schematic diagram for exterior diffuse sound field excitation.

Fig. 4(c) is the detail view of the elastic mounting. Different rubber mounts result in different restraint stiffness and damping. Soft material is needed for approximating the free boundary conditions.

In the investigation of airborne noise, exterior diffuse sound field excitation was also considered in the design. The diffuse sound field is an ideal sound field that never exists, but it is commonly used in research. In the experiment, the diffuse sound field can be approximated by the reverberation chamber, so the test bench was designed for mounting on the window of a standard reverberation chamber. As shown by Fig. 5, with the help of a concrete frame, the flexible panel is excited by the diffuse sound field while the test bench is outside the reverberation chamber. Therefore, there are thread holes around the front edges for fastening the test bench to the concrete frame and on the top for lifting the test bench to a certain height.

2.4. Final Design Overview

In consideration of size, weight and construction, the final design was determined, as shown in Fig. 6. The equipment occupies around 2 m^3 and weighs about 2.5 tons. The rigid walls are no less than 200 mm in thickness. The cavity inside is 0.596 m^3, shaped like a pentagonal prism. It is similar to the one shown in Fig. 3, but has a small step of 40 mm around the opening of the cavity, which was modified for the construction. All dimensions of the cavity are annotated in Fig. 6.

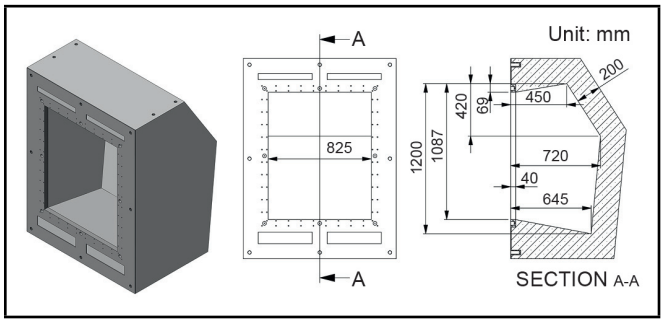

Figure 6. Final design of Noise-Box with cavity dimensions.

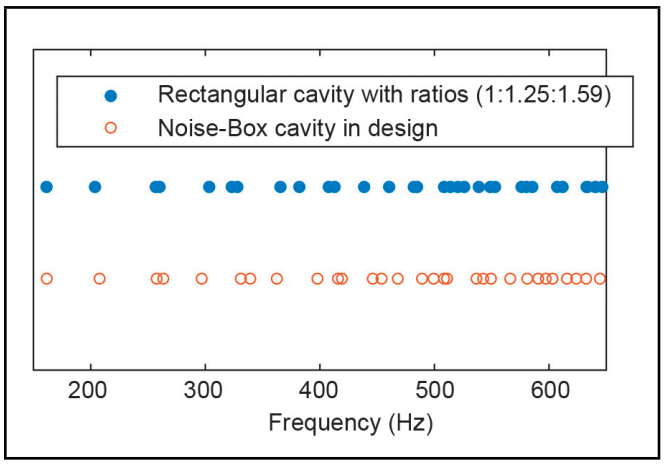

Figure 7. Distribution of natural frequencies up to 650 Hz.

The shape was optimized according to the frequency spacing index ψ(defined by Eq. (1)) using the optimization strategy introduced in Section 2.2. In the optimization, the air density and the sound speed were assumed to be $\rho = 1.2$ kg/m^3 and $c = 343$ m/s, and the cut-off frequency $f_c = 647$ Hz (based on Eq. (5)) was used. The natural frequencies were obtained from the modal analysis by the FEM via COMSOL. After the optimization, the final frequency spacing index is given by $\psi = 1.57$, smaller than the value ($\psi = 1.71$) of a rectangular room that has the same volume ($V = 0.596$ m^3) and the recommended dimensional ratios (1:1.26:1.59). The comparison of their eigenfrequency distributions is shown in Fig. 7, which also illustrates that the first eigenfrequency of the final design is around 160 Hz.

3. CHARACTERIZATION OF THE TEST BENCH

This section characterizes the modal property, sound absorption and spatial variation/diffuseness of the interior cavity. The characterization is conducted in two parts. One part is the measurement over the physical test bench, and the other is the prediction by numerical models. Indeed, both solutions have certain assumptions and simplifications. In order to have a better knowledge of the test bench, the two sets of results were obtained and compared.

3.1. Experimental Set-up

The same experimental set-up was used for the following three tests to characterize the cavity inside the Noise-Box:

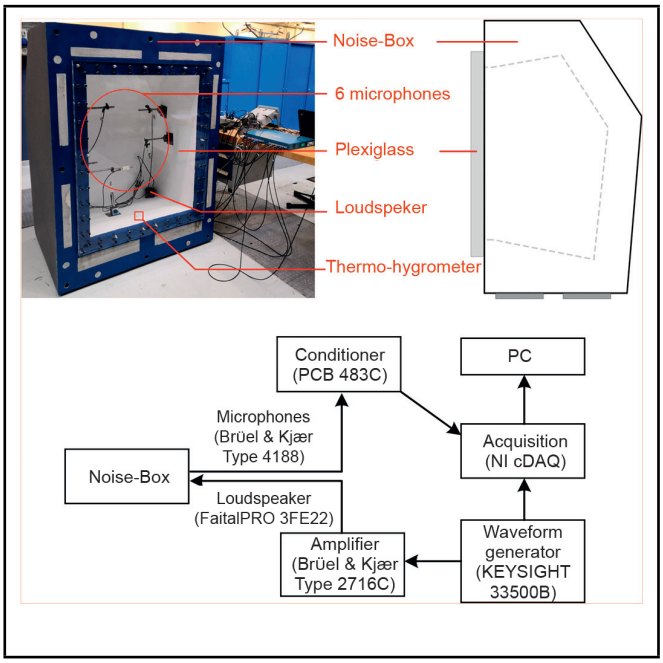

Figure 8. Photograph and schematic of the experimental set-up

1. experimental modal analysis;
2. reverberation time measurement; and,
3. inner pressure field spatial variation measurement.

Fig. 8 shows the photograph and schematic of the set-up. The opening of the Noise-Box is closed by a transparent plexiglass plate of 25 mm in thickness. A loudspeaker (FaitalPRO 3FE22) is at the right corner of the cavity, exciting the acoustic field. Six microphones (Brüel & Kjær Type 4188) are placed inside at six different positions that are neither too close to each other nor too close to the walls. A thermo-hygrometer (INKBIRO IBS-TH1 Mini) is on the floor, monitoring the temperature and humidity inside the cavity. As shown in the schematic, the signal generated by the waveform generator (KEYSIGHT 33500B) is output to two instruments. One is to the power amplifier (Brüel & Kjær Type 2716C), where the signal is amplified before input to the loudspeaker. The other is to the acquisition system (NI cDAQ), so that the input signal is recorded. Additionally, the signals from microphones are acquired with the aid of the sensor signal conditioner (PCB 483C).

3.2. Numerical Models

The experiments can be simulated using numerical models. Numerical simulation is an important part in the development of the Noise-Box. The simulation can be conducted in the design stage for the design optimization, before the experiment for a better experimental design or after the experiment for the model updating and further predictions. In this paper, FEM is used for the numerical investigations, via the commercial software COMSOL.

The FE models of the Noise-Box cavity are shown in Fig. 9. They were modelled using quadratic Lagrange elements, and the element sizes were determined by guaranteeing a good convergence of the results in the frequency range of interest. Fig. 9(a) shows the 3D FE model with the element size no

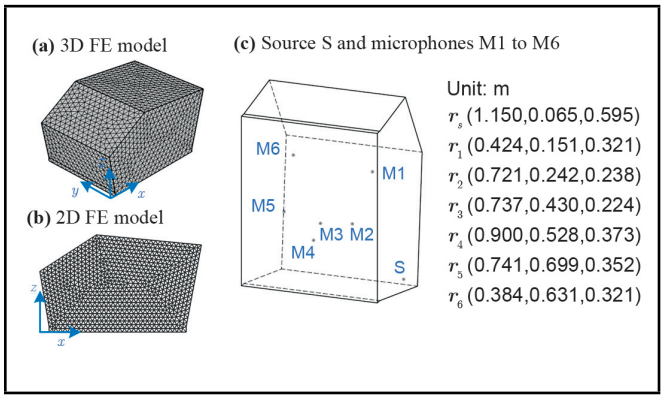

Figure 9. Models for numerical simulations.

larger than 0.056 m (more than 6 elements per wavelength up to 1000 Hz). Fig. 9(b) shows the corresponding 2D model with the element size no larger than 0.034 m (more than 10 elements per wavelength up to 1000 Hz). Because of the two parallel walls, the 2D model is available and can be used to represent the 3D cavity. For example, in the modal analysis, if the cavity is considered as a rigid-walled cavity, its modes satisfy:[1]

$$p(x,y,z) = p(x,z)\cos\left(\frac{n_y \pi y}{L_y}\right); \tag{6}$$

and its natural frequencies are given by:

$$f_{3D} = \sqrt{f_{2D}^2 + \left(\frac{c}{2}\frac{n_y}{L_y}\right)^2}, n_y = 0,1,\ldots; \tag{7}$$

where n_y is the order of the standing wave in y direction, f_{3D} denotes the natural frequency of the 3D cavity, f_{2D} is the natural frequency of the 2D model, $p(x,y,z)$ is the pressure distribution. Though it is optional to directly use the 3D model, the proof of the 2D model is meaningful, since using the 2D model significantly saves the computational time and memory, especially for higher frequencies.

Corresponding to the positions of microphones and a loudspeaker in the experiment (see Fig. 8), the measurement and source points are specified in the 3D model, as shown in Fig. 9(c). Given a unit input to the source S, the frequency responses at the measurement points M1 to M6 can be predicted using the model. Then, the simulation results are comparable with the experimental ones.

3.3. Modal Characteristics

Experimental and numerical approaches are combined together to identify the modal characteristics of the interior acoustic field. The experimental modal analysis was performed using the experimental set-up shown in Fig. 8, where the loudspeaker was driven by a white noise signal up to 3,000 Hz. A sampling frequency of 12800 Hz was used, and the signals were recorded for 1050 sec. In the signal processing, a Hanning window of 15 sec was applied. As a result, the average was done over 70 samples and the frequency resolution is 0.0667 Hz. Then, according to the transfer functions between sound pressures measured by the microphones and the input signal, the first 31 natural frequencies were identified by the peak-picking method, and they are listed as f_{exp} in Table 1. During the test, the temperature and humidity inside the cavity were recorded as (24.16 ± 0.01)°C and $(75.5\pm0.13\%)$ RH, respectively.

Correspondingly, numerical modal analyses were conducted based on the COMSOL 3D and the COMSOL 2D FE models, respectively, as shown in Fig. 9(a) and Fig. 9(b). According to the experimental temperature 24.16°C, the air density and acoustic speed were given by: $\rho = 1.1875$ kg/m^3 and $c = 345.63$ m/s. For the results from the COMSOL 2D model, Eq. (7) was used to calculate the eigenfrequencies from f_{2D} to f_{3D}. In order to distinguish the two sets of natural frequencies, the set of COMSOL 3D is denoted as $f_{3D}^{(a)}$ and the other is denoted as $f_{3D}^{(b)}$. The two sets of numerical results are listed in Table 1. A good agreement can be observed between them, verifying the equivalence in accuracy for the two numerical models in modal analysis. Meanwhile, this process also proves that the 2D model is more efficient. In this case, using the 3D and 2D FE models with the element sizes the same as they are shown in Fig. 9(a) and Fig. 9(b), respectively, the 3D model has 10288 degrees of freedom (DOF) and requires 260 sec for the eigenfrequency analysis, while the 2D one has only 862 DOF and computes for only 6 sec on the same computer (Windows system with 4 cores of Intel(R) Core(TM) i7-6700 CPU @ 3.40GHz).

When the numerical results are compared with the experimental ones, Table 1 shows that the relative prediction error in natural frequency is less than 0.6%. The good agreement indicates that the results from both the experiment and the simulation can be used to represent the modal characteristics of the Noise-Box cavity. However, it should be noticed that the current numerical models have neglected the inevitable parameter uncertainty in the geometric and material properties of the Noise-Box cavity. For a more representative FE model, the model robustness can be further studied.[52–54]

3.4. Reverberation Time and Sound Absorption

Regarding the sound absorption of a room, two parameters are commonly used: the reverberation time T_{60} and the average absorption coefficient $\bar{\alpha}$. The two parameters are closely related to each other, and the Sabine formula is provided that:[40]

$$T_{60} = \frac{0.161V}{\bar{\alpha}S}; \tag{8}$$

where V is volume of the room, S is the total surface area. With respect to the Noise-Box, the reverberation time T_{60} was obtained from measurement, and the absorption coefficient $\bar{\alpha}$ was derived according to Eq. (8), with the volume of the cavity $V = 0.596$ m^3 and surface area of the cavity $S = 4.26$ m^2. The considered frequencies are all the 1/3 octave bands within 141 Hz to 7080 Hz.

Interrupted noise method was used to measure the reverberation time, following the instructions of ISO 3382-2.[43] For each measurement, white noise covering the bands of interest was generated as input to build a steady-state acoustic field inside the cavity. The excitation had lasted for 10 sec before it was stopped. Then, after the signal switched off, the responses were continuously recorded for 20 sec, so that the

Table 1. Numerical and experimental natural frequencies of the Noise-Box cavity.

Mode order	Experiment f_{exp} (Hz)	COMSOL 3D $f_{3D}^{(a)}$ (Hz)	COMSOL 2D				$\frac{f_{3D}^{(a)}-f_{\text{exp}}}{f_{\text{exp}}} \times 100\%$
			2D modes		n_y	$f_{3D}^{(b)}$ (Hz)	
			Order	f_{2D} (Hz)			
1	0	0	1	0	0	0	–
2	162.87	163.05	2	163.05	0	163.05	0.11%
3	208.93	209.47	1	0	1	209.47	0.26%
4	259.47	259.65	3	259.65	0	259.65	0.07%
5	265.53	265.45	2	163.05	1	265.45	-0.03%
6	300.03	299.19	4	299.19	0	299.19	-0.28%
7	333.67	333.61	3	259.65	1	333.61	-0.02%
8	342.60	341.86	5	341.86	0	341.86	-0.22%
9	366.07	365.23	4	299.19	1	365.23	-0.23%
10	401.40	400.94	5	341.86	1	400.93	-0.11%
11	418.93	418.95	1	0	2	418.95	0.00%
12	423.17	422.47	6	422.46	0	422.46	-0.16%
13	450.27	449.56	2	163.05	2	449.56	-0.16%
14	459.60	457.29	7	457.29	0	457.29	-0.50%
15	471.93	471.55	6	422.46	1	471.54	-0.08%
16	494.50	492.89	3	259.65	2	492.88	-0.33%
17	505.07	502.99	7	457.29	1	502.98	-0.41%
18	512.13	512.24	8	512.24	0	512.24	0.02%
19	516.40	514.82	4	299.19	2	514.81	-0.31%
20	542.70	540.74	5	341.86	2	540.73	-0.36%
21	549.40	546.57	9	546.56	0	546.56	-0.52%
22	551.87	553.42	8	512.24	1	553.42	0.28%
23	570.07	570.32	10	570.31	0	570.31	0.04%
24	586.90	585.34	9	546.56	1	585.33	-0.27%
25	594.73	594.99	6	422.46	2	594.97	0.04%
26	604.93	601.64	11	601.63	0	601.63	-0.54%
27	606.33	607.58	10	570.31	1	607.56	0.21%
28	623.00	620.20	7	457.29	2	620.19	-0.45%
29	630.93	628.44	1	0	3	628.42	-0.40%
30	638.83	637.07	11	601.63	1	637.05	-0.28%
31	651.63	649.25	2	163.05	3	649.23	-0.37%

cavity reached the background noise level. A total of 20 measurements was performed, and they were averaged with the preferred way,[43] where the ensemble average of the squared sound pressure decays was used. Due to the relatively low sound pressure level (SPL) in the low frequency range, the T20 measurement method was used. In this case, the decay curves started at least 35 dB above the background noise for all the 1/3 octave bands of interest. The reverberation time is given by:

$$T_{60} = 60/d; \tag{9}$$

where d is the decay rate in decibels per second. It is determined from the slope of the least-squares fit line of the decay curve from 5 dB to 25 dB below the steady-state level. Fig. 10 shows an example (measured by microphone M1 for 1000 Hz 1/3 octave band) in the data processing that applies the T20 measurement method.

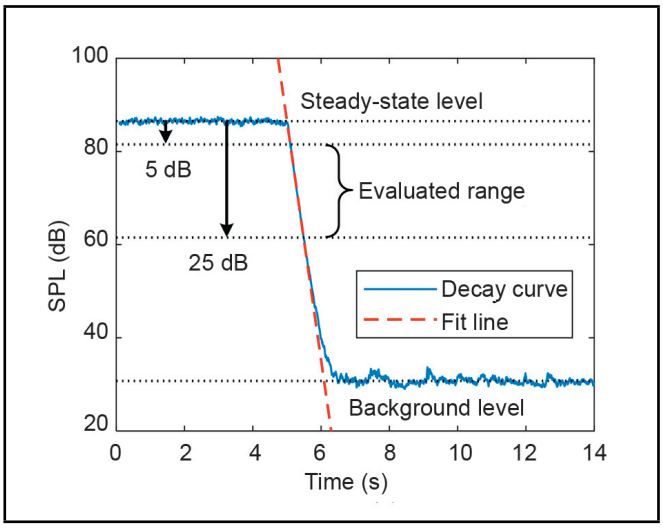

Figure 10. SPL at M1 for 1000 Hz 1/3 octave band in the T20.

For every 1/3 octave band whose central frequency is between 160 Hz to 6300 Hz, the reverberation time corresponding to each of the six microphones (from M1 to M6 as shown in Fig. 8 and Fig. 9) was obtained following the same procedures. The results are listed in Table 2. f_m denotes the 1/3 octave mid-band frequency, and T_{60,M_i} denotes the reverberation time measured at microphone position Mi. The average and standard deviation of the reverberation time are calculated over the six microphone positions for each band using the equations:

$$T_{60} = \frac{1}{n_M}\sum_{i=1}^{n_M} T_{60,Mi} \quad \text{and}$$
$$\sigma_T = \sqrt{\frac{1}{n_M - 1}\sum_{i=1}^{n_M}\left(T_{60,Mi} - T_{60}\right)^2}; \tag{10}$$

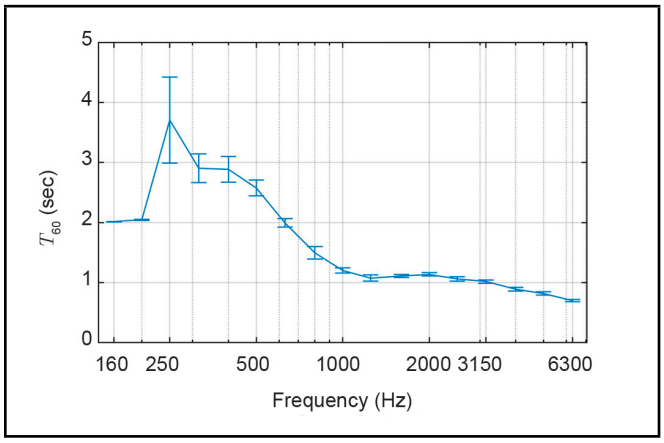

Figure 11. Reverberation time T_{60} with its standard deviation σ_T.

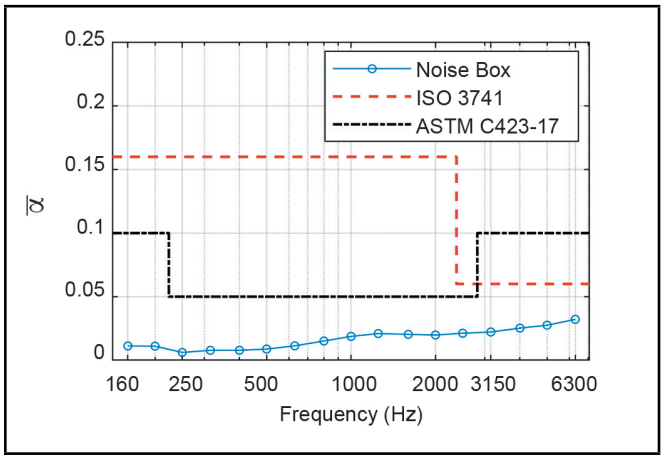

Figure 12. Average absorption coefficient $\bar{\alpha}$ of the Noise-Box.

with the number of microphones $n_M = 6$.

Fig 11 shows the change of the reverberation time T_{60} with the increase of band frequency, where the standard deviation σ_T is plotted using an error bar. As the figure shows, except the first two bands, the reverberation time tends to decrease when the frequency increases, which indicates a higher energy dissipation.

In addition, the sound absorption coefficient $\bar{\alpha}$ has been calculated according to Eq. (8) and listed in Table 2. Fig. 12 shows the comparison between the absorption coefficient $\bar{\alpha}$ of the Noise-Box and the corresponding upper limit of reverberation test room in ISO 3471[41]and ASTM C423-17.[55] It can be observed that the sound absorption of the Noise-Box cavity is much smaller than the upper limit of the standard reverberation room. On the other hand, the absorption coefficient $\bar{\alpha}$ can be used to update the wall impedance of the numerical models. Assumed that the sound absorption is uniform over all walls and that the sound transmission through walls is negligible, the wall impedance of all the cavity boundaries can be updated with:[56]

$$Z = \rho c \frac{1+\sqrt{1-\bar{\alpha}}}{1-\sqrt{1-\bar{\alpha}}}. \tag{11}$$

Then, the updated numerical model can be used to analyze the frequency response of the cavity with the damping effect considered.

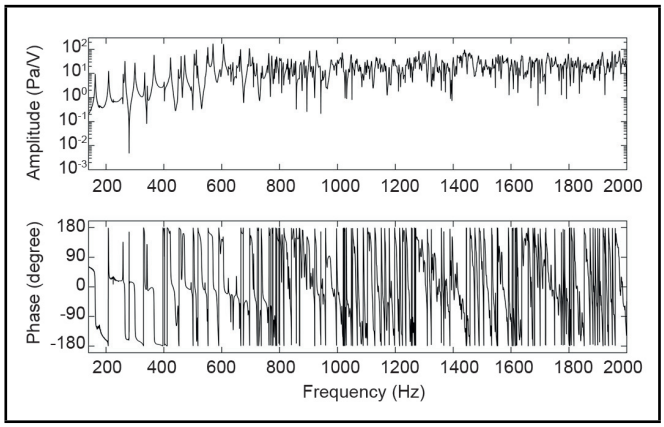

Figure 13. Experimental transfer function for M1.

3.5. Sound Field Diffuseness

Fig. 13 shows the experimental transfer function between the sound pressure measured by one of the microphones (M1 in Fig. 9) and the input signal generated by the waveform generator (see Fig. 8). It should be noted that the adjacent natural frequencies become very close when they are above the defined cut-off frequency $f_c \approx 650$ Hz. As the frequency increases, the modal density and the modal overlap increase. Meanwhile, the sound field becomes more diffuse or spatially uniform. Therefore, the diffuseness characteristic becomes more important at higher frequencies. It determines whether we can consider the sound field to be uniform or use the Noise-Box as a reverberation room. It also relates to the division of solution frequency ranges for acoustic/vibroacoustic problems.[11]

There are several quantifiers for the field diffuseness.[57] Two quantifiers are used here to characterize the inner sound field of the Noise-Box. One of the quantifiers is the mode count or the modal overlap in 1/3 octave band. When the modal overlap goes too high as the frequency increases, counting the modes with the experimental transfer function becomes impractical. Accordingly, the validated numerical models were used to identify the modes. Since the increase of frequency requires a much larger model size (to keep at least 6 elements per wavelength) and much more extracting modes (up to 7080 Hz), the 2D FE model was used instead of the 3D one, which has saved a lot of computational memory and time. Table 3 lists the mode count N, the modal density n and the modal overlap M in each 1/3 octave band centered from 160 Hz to 6300 Hz. The modal density n is defined as the number of modes per Hz and calculated by dividing the mode count N with the corresponding bandwidth. The modal overlap M is evaluated by $M = 2.2n/T_{60}$, using reverberation time T_{60} from experiment (as listed in Table 2). Then, the criteria are considered. The less rigorous one defines the limit to diffuse sound field as more than 20 modes per third octave band. It can be observed from Table 3 that the cut-off frequency is between 630 Hz to 800 Hz. Thus, it is valid to use Eq. (5) to evaluate the cut-off frequency with $f_c \approx 650$ Hz. The restrictive one known as the Schroeder frequency corresponds to the modal overlap of no less than 3. Table 3 indicates that this frequency is between 2500 Hz to 3150 Hz, which conforms to the calculation based on Eq. (4), having $f_s = 2669$ Hz. There is a wide frequency range between f_c and f_s. It can be reasonable to consider this range as a transition between the modal region $f < f_c$ and the

Table 2. Reverberation time T_{60} and average absorption coefficient $\bar{\alpha}$ of the Noise-Box.

f_m (Hz)	Reverberation time (sec)								$\bar{\alpha}$
	$T_{60,\,M1}$	$T_{60,\,M2}$	$T_{60,\,M3}$	$T_{60,\,M4}$	$T_{60,\,M5}$	$T_{60,\,M6}$	T_{60}	σ_T	
160	2.02	2.02	2.02	2.02	2.02	2.02	**2.02**	0.00	**0.011**
200	2.05	2.05	2.03	2.04	2.05	2.05	**2.04**	0.01	**0.011**
250	3.30	4.10	5.13	3.14	3.47	3.11	**3.71**	0.71	**0.006**
315	2.69	2.65	3.33	3.01	2.73	3.03	**2.90**	0.24	**0.008**
400	2.57	3.02	3.09	3.00	3.03	2.61	**2.89**	0.21	**0.008**
500	2.37	2.79	2.52	2.59	2.69	2.49	**2.58**	0.13	**0.009**
630	1.98	1.99	1.89	2.11	2.06	1.93	**1.99**	0.07	**0.011**
800	1.47	1.50	1.43	1.72	1.42	1.44	**1.50**	0.10	**0.015**
1000	1.17	1.23	1.15	1.28	1.21	1.19	**1.20**	0.04	**0.019**
1250	1.14	1.15	1.07	1.04	1.03	1.03	**1.08**	0.05	**0.021**
1600	1.10	1.12	1.12	1.15	1.09	1.07	**1.11**	0.03	**0.020**
2000	1.12	1.12	1.10	1.19	1.15	1.15	**1.14**	0.03	**0.020**
2500	1.07	1.06	1.03	1.08	1.12	1.02	**1.06**	0.03	**0.021**
3150	1.02	1.05	0.96	1.00	1.03	1.03	**1.02**	0.03	**0.022**
4000	0.86	0.92	0.90	0.92	0.84	0.92	**0.89**	0.03	**0.025**
5000	0.82	0.82	0.83	0.86	0.77	0.82	**0.82**	0.03	**0.028**
6300	0.69	0.72	0.71	0.71	0.67	0.70	**0.70**	0.02	**0.032**

Table 3. Mode count, modal density and modal overlap of the Noise-Box cavity.

f_m (Hz)	Mode count N	Modal density n(Hz^{-1})	Modal overlap M
160	1	0.027	0.03
200	1	0.022	0.02
250	2	0.034	0.02
315	3	0.041	0.03
400	4	0.043	0.03
500	10	0.087	0.07
630	17	0.116	0.13
800	31	0.169	0.25
1000	55	0.240	0.44
1250	106	0.366	0.75
1600	204	0.551	1.09
2000	392	0.852	1.65
2500	761	1.312	2.72
3150	1476	2.022	4.38
4000	2908	3.161	7.79
5000	5663	4.924	13.23
6300	11238	7.697	24.16

highly diffuse Schroeder region $f > f_s$. The parameters listed in Table 3 also provide a reference for considering whether to use FEM or Statistical Energy Analysis (SEA) methods to analyze the acoustic field. If $M > 1$ is considered as a prerequisite for applying SEA, the frequency range should be $f >$ 1250 Hz.

The other quantifier is the spatial uniformity or variation of the sound pressure field. In the experiment, sound pressures at the six microphone positions were measured, while the inner acoustic field was at the steady state excited by the white noise up to 8000 Hz. The SPLs among the six positions are compared for every 1/3 octave band, as shown in Fig. 14. Corresponding standard deviations σ_M over the six positions can be used for the quantification, and the results are shown in Fig. 15. Some cases require that $\sigma_M \leq 1.5$ dB for the sound field to be considered as uniform,[57] while the ISO 3471[41] has a more precise limit to qualify the reverberation test room. Fig. 15 includes the maximum allowable lines from both the 1.5 dB limit and the qualification limit from the ISO 3471. However, it should be noticed that the provided qualification limit from

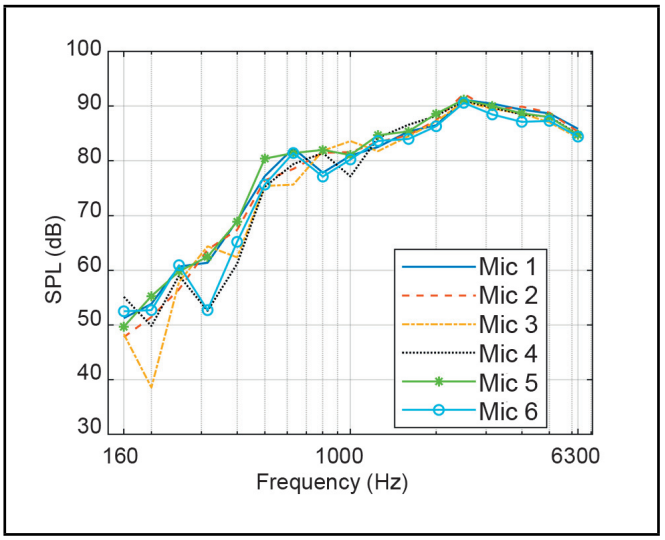

Figure 14. SPLs measured by the 6 microphones inside Noise-Box.

the ISO 3471 is originally for the sound sources instead of the microphones, and that some other requirements with respect to the microphone and sound source positions are not able to be utilized due to the small size of the Noise-Box. According to these criteria, it can be observed from Fig. 15 that the starting frequency for the diffuse field is between 1000 Hz to 1250 Hz, or between 2500 Hz to 3150 Hz. The limit frequency satisfying the ISO 3471 is consistent with the Schroeder frequency $f_s = 2669$ Hz. Therefore, it is believed that the sound field is sufficiently diffused in the frequency range higher than the 2500 Hz 1/3 octave band. Nevertheless, it is practical to consider the Noise-Box as a small reverberation room when the frequencies are higher than the 1000 Hz 1/3 octave band.

4. CONCLUSIONS

A test bench named Noise-Box has been designed and built. It was targeted for benchmarking the numerical methods for vibroacoustic analysis and testing the interior noise control techniques for vehicles. In the test bench, the cabin was simplified into a plate-cavity system composed of six rigid concrete walls and one flexible panel. Its simple geometry and physics were

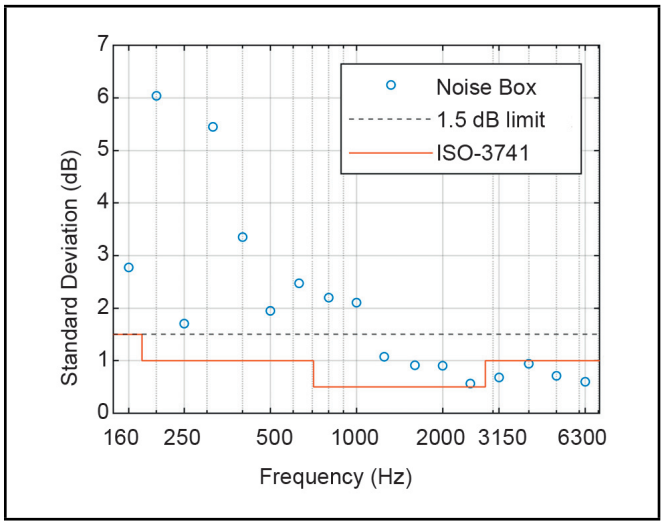

Figure 15. Standard deviation of SPLs over the 6 microphones inside Noise-Box.

to make sure that the vibroacoustic tests performed on it could be accurately reproduced by numerical models. This work introduced the design of the test bench and specified the characteristics of the acoustic field inside. Meanwhile, the methods used in the process were demonstrated. The results are important for future application of the test bench and the methods are instructive for developing similar facilities.

The shape of the cavity was inspired from a real car compartment and simplified as a pentagonal prism. The two side walls are pentagonal and parallel while the others are rectangular. This design enables the 3D numerical model to be reduced to 2D if necessary. The dimensional ratios of the cavity were specially determined to reach a more diffuse sound field in the low frequency range, by evaluating and observing the eigenfrequency distribution of the acoustic field. A uniform eigenfrequency distribution in the low frequency range was preferred, which is quantified by the frequency spacing index ψ, the mean square of the deviations of the distances between subsequent modes. With a smaller index ψ, the final design showed a more uniform eigenfrequency distribution than the rectangular reverberation rooms of the same volume 0.596 m^3. Then, for mounting the flexible panel, the Noise-Box was equipped with different holes for rigid and elastic supports. Considering the possibility for exterior diffuse sound field excitation, screw holes were also prepared for moving and installing it into a reverberation chamber. Finally, the Noise-Box, which was formed by concrete walls with no less than 200 mm in thickness, occupied around 2 m^3 and weighed about 2.5 tons.

The interior acoustic field of the Noise-Box test bench has been characterized numerically or experimentally for its modal property, sound absorption and field diffuseness. The cavity modes under 650 Hz were identified numerically and experimentally. The results agree well with each other. The 3D and 2D FE models have been proven accurate for modal analysis. The reverberation time for 1/3 octave bands within 141 Hz to 7080 Hz was measured using the T20 measurement method and the average absorption coefficient was calculated based on the Sabine formula. It is found that the sound absorption of room inside is sufficiently small to meet the requirement of a reverberation room. In the evaluation of sound field diffuseness, several quantifiers were used. It is known that the sound field becomes diffuse as the frequency increases, but the lower limit needs to be determined. The mode count of 20 modes per third octave band accords with the cut-off frequency 650 Hz. Below this frequency, the acoustic field was dominated by the modal properties. The modal overlap factor no less than 1 and 3 respectively advocates the lower limit larger than 1250 Hz and 2500 Hz, where the latter agrees with the Schroeder frequency 2669 Hz, above which the sound field was ideally diffuse. Additionally, the spatial standard deviation of the sound pressure levels indicated two other limits, i.e., 1000 Hz and 2500 Hz. By comparison, it can be concluded that there is a transition for the diffuse level from 650 to 2500 Hz.

REFERENCES

[1] Fahy, F. Advanced Applications in Acoustics, *Noise and Vibration*, Spon Press, London, (2004). https://doi.org/10.1201/9781315273396.

[2] Genuit, K., 2009, "Vehicle Interior Noise - Combination of Sound, Vibration and Interactivity," *Sound Vib.*, **43**(12), pp. 8–13.

[3] Zevitas, C.D., Spengler, J.D., Jones, B., McNeely, E., Coull, B., Cao, X., Loo, S.M., Hard, A.K. and Allen, J.G. Assessment of noise in the airplane cabin environment, *Journal of Exposure Science and Environmental Epidemiology*, **28**, 568–578, (2018). https://doi.org/10.1038/s41370-018-0027-z.

[4] Soeta, Y. and Shimokura, R. Survey of interior noise characteristics in various types of trains, *Applied Acoustics*, **74**, 1160–1166, (2013). https://doi.org/10.1016/j.apacoust.2013.04.002.

[5] Wilby, J.F. Aircraft interior noise, *Journal of Sound and Vibration*, **190**, 545–564, (1996). https://doi.org/10.1006/jsvi.1996.0078.

[6] Qatu, M.S. Recent research on vehicle noise and vibration, *International Journal of Vehicle Noise and Vibration*, **8**, 289–301, (2012). https://doi.org/10.1504/IJVNV.2012.051536.

[7] Dobrzynski, W. Almost 40 years of airframe noise research: What did we achieve?, *Journal of Aircraft*, **47**, 353–367, (2010). https://doi.org/10.2514/1.44457.

[8] Bein, T., Elliott, S., Ferralli, L., Casella, M., Meschke, J., Saemann, E.-U., Nielsen, F.-K. and Kropp, W. Integrated Solutions for Noise & Vibration Control in Vehicles, *Procedia - Social and Behavioral Sciences*, **48**, 919–931, (2012). https://doi.org/10.1016/j.sbspro.2012.06.1069.

[9] Fischer, J., Behrendt, M., Lieske, D. and Albers, A. Measurement and analysis of the interior noise and the transfer path of acoustic phenomena into the driver cabin of a battery electric vehicle, in: INTERNOISE 2014 - 43rd International Congress on Noise Control Engineering: Improving the World Through Noise Control, Melbourne, Austrialia, (2014): p. 110.

[10] Pozar, M. and Cook, H.E. On determining the relationship between vehicle value and interior noise, in: SAE Technical Papers, SAE International, (1998). https://doi.org/10.4271/980621.

[11] Hambric, S.A., Sung, S.H. and Nefske, D.J. Engineering Vibroacoustic Analysis: Methods and Applications, John Wiley & Sons, Ltd, Chichester (UK), (2016). https://doi.org/10.1002/9781118693988.

[12] Molares, A.R. and Sobreira-Seoane, M.A. Benchmarking for acoustic simulation software, in: Proceedings - European Conference on Noise Control, (2008): pp. 3601–3606. https://doi.org/10.1121/1.2934429.

[13] Néjade, A. C-valor — a vibro-acoustic software validation tool, *Sound and Vibration*, **44**, 5–7, (2010).

[14] Hornikx, M., Kaltenbacher, M. and Marburg, S. A platform for benchmark cases in computational acoustics, *Acta Acustica United with Acustica*, **101**, 811–820, (2015). https://doi.org/10.3813/AAA.918875.

[15] Milo D. Dahl Fourth Computational Aeroacoustics (CAA) Workshop on Benchmark Problems, in: Proceedings of a Conference Held at Ohio Aerospace Institute and Cosponsored by the Ohio Aerospace Institute, Cleveland, Ohio, (2003). https://www.math.fsu.edu/CAA4/problems.html (accessed April 15, 2021).

[16] Benchmark Platform on Computatinal Methods for Archtectural/Environmental Acoustics. http://news-sv.aij.or.jp/kankyo/s26/AIJ-BPCA/index.html (accessed April 15, 2021).

[17] European Acoustics Association: Benchmark Cases for Computational Acoustics. https://eaa-bench.mec.tuwien.ac.at/main/ (accessed April 15, 2021).

[18] Del Rey, R., Alba, J., Bertó, L. and Gregori, A. Small-sized reverberation chamber for the measurement of sound absorption, *Materiales de Construccion*, **67**, 139, (2017). https://doi.org/10.3989/mc.2017.07316.

[19] Vivolo, M. Vibro-acoustic Characterization of Lightweight Panels by using a Small Cabin, KU Leuven, Ph.D. Thesis, (2013).

[20] Cheer, J. Active control of the acoustic environment in an automobile cabin, University of Southampton, Ph.D. Thesis, (2012).

[21] Ripamonti, F., Giampà, A., Giona, R., Liu, L. and Corradi, R. Numerical and experimental study of an active control logic for modifying the acoustic performance of single-layer panels, *Journal of Sound and Vibration*, **520**, 116608, (2022). https://doi.org/10.1016/j.jsv.2021.116608.

[22] Liu, Z.S., Lee, H.P. and Lu, C. Passive and active interior noise control of box structures using the structural intensity method, *Applied Acoustics*, **67**, 112–134, (2006). https://doi.org/10.1016/j.apacoust.2005.04.010.

[23] Dammak, K., Koubaa, S., El Hami, A., Walha, L. and Haddar, M. Numerical modelling of vibro-acoustic problem in presence of uncertainty: Application to a vehicle cabin, *Applied Acoustics*, **144**, 113–123, (2019). https://doi.org/10.1016/j.apacoust.2017.06.001.

[24] Georgiev, V.B. Simplified reduced-scale modelling of vehicle interior noise, Loughborough University, Ph.D. Thesis, (2006).

[25] Marburg, S., Beer, H.J., Gier, J., Hardtke, H.J., Rennert, R. and Perret, F. Experimental verification of structural-acoustic modelling and design optimization, *Journal of Sound and Vibration*, **252**, 591–615, (2002). https://doi.org/10.1006/jsvi.2001.4037.

[26] Dowell, E.H. and Voss, H.M. The effect of a cavity on panel vibration, *AIAA Journal*, **1**, 476–477, (1963). https://doi.org/10.2514/3.1568.

[27] Lyon, R.H. Noise reduction of rectangular enclosures with one flexible wall, *The Journal of the Acoustical Society of America*, **35**, 1791–1797, (1963). https://doi.org/10.1121/1.1918822.

[28] Dowell, E.H., Gorman, G.F. and Smith, D.A. Acoustoelasticity: General theory, acoustic natural modes and forced response to sinusoidal excitation, including comparisons with experiment, *Journal of Sound and Vibration*, **52**, 519–542, (1977). https://doi.org/10.1016/0022-460X(77)90368-6.

[29] Al-Bassyiouni, M. and Balachandran, B. Sound transmission through a flexible panel into an enclosure: structural–acoustics model, *Journal of Sound and Vibration*, **284**, 467–486, (2005). https://doi.org/10.1016/j.jsv.2004.06.040.

[30] Zhang, H., Shi, D., Zha, S. and Wang, Q. Parameterization study on the moderately thick laminated rectangular plate-cavity coupling system with uniform or non-uniform boundary conditions, *Composite Structures*, **194**, 537–554, (2018). https://doi.org/10.1016/j.compstruct.2018.04.034.

[31] Zhang, H., Shi, D., Zha, S. and Wang, Q. Vibro-acoustic analysis of the thin laminated rectangular plate-cavity coupling system, *Composite Structures*, **189**, 570–585, (2018). https://doi.org/10.1016/j.compstruct.2018.01.099.

[32] Xie, X., Zheng, H. and Qu, Y. A variational formulation for vibro-acoustic analysis of a panel backed by an irregularly-bounded cavity, *Journal of Sound and Vibration*, **373**, 147–163, (2016). https://doi.org/10.1016/j.jsv.2016.03.003.

[33] Mi, Y. and Zheng, H. An interpolation method for coupling non-conforming patches in isogeometric analysis of vibro-acoustic systems, *Computer Methods in Applied Mechanics and Engineering*, **341**, 551–570, (2018). https://doi.org/10.1016/j.cma.2018.07.002.

[34] Shi, S.X., Jin, G.Y. and Liu, Z.G. Vibro-acoustic behaviors of an elastically restrained double-panel structure with an acoustic cavity of arbitrary boundary impedance, *Applied Acoustics*, **76**, 431–444, (2014). https://doi.org/10.1016/j.apacoust.2013.09.008.

[35] Chen, Y., Jin, G., Shi, S. and Liu, Z. A General Analytical Method for Vibroacoustic Analysis of an Arbitrarily Restrained Rectangular Plate Backed by a Cavity With General Wall Impedance, *Journal of Vibration and Acoustics*, **136**, (2014). https://doi.org/10.1115/1.4027136.

[36] Xie, X., Yang, H. and Zheng, H. A weak formulation for interior acoustic analysis of enclosures with inclined walls and impedance boundary, Wave Motion. (2016). https://doi.org/10.1016/j.wavemoti.2016.04.012.

[37] Liu, Z., Fard, M. and Davy, J.L. Acoustic properties of the porous material in a car cabin model, in: Proceedings of the 23rd International Congress on Sound and Vibration, ICSV 2016, Athensm, Greece, (2016).

[38] Gorman, R. and Krylov, V. Investigation of acoustic properties of vehicle compartments using reduced-scale simplified models, in: Proceedings of the Institute of Acoustics, (2004): pp. 37–48.

[39] Fahy, F. and Gardonio, P. Sound and Structural Vibration: radiation, transmission and response, Elsevier, Amsterdam, (2007). https://doi.org/10.1016/B978-0-12-373633-8.X5000-5.

[40] Kinsler, L., Frey, A., Coppens, A. and Sanders, J. Fundamentals of acoustics, 4th ed., John Wiley & Sons, Inc., New York, (1999).

[41] ISO 3741 Acoustics — Determination of sound power levels and sound energy levels of noise sources using sound pressure — Precision methods for reverberation test rooms., (2010). https://www.iso.org/standard/52053.html.

[42] ISO 10140-5 Acoustics — Laboratory measurement of sound insulation of building elements — Part 5: Requirements for test facilities and equipment, (2021). https://www.iso.org/standard/79482.html.

[43] ISO 3382-2 Acoustics — Measurement of room acoustic parameters — Part 2: Reverberation time in ordinary rooms, (2008). https://www.iso.org/standard/36201.html.

[44] Hasan, M. and Hodgson, M. Effectiveness of reverberation room design: Room size and shape and effect on measurement accuracy, in: Proceedings of the 22nd International Congress on Acoustics, (2016).

[45] Le Bot, A. and Cotoni, V. Validity diagrams of statistical energy analysis, *Journal of Sound and Vibration*, **329**, 221–235, (2010). https://doi.org/10.1016/j.jsv.2009.09.008.

[46] Lafont, T., Totaro, N. and Bot, A. Le Review of statistical energy analysis hypotheses in vibroacoustics, Proceedings of the Royal Society A: Mathematical, *Physical and Engineering Sciences*, **470**, (2014). https://doi.org/10.1098/rspa.2013.0515.

[47] Błaszak, M.A. Acoustic design of small rectangular rooms: Normal frequency statistics, *Applied Acoustics*, **69**, 1356–1360, (2008). https://doi.org/10.1016/j.apacoust.2007.10.005.

[48] Hernandez, D., Liu, E.J., Huang, J.H. and Liu, Y.C. Design and Construction of a Small Reverberation Chamber Applied to Absorption and Scattering Acoustic Measurements, *Advanced Materials Research*, **1077**, 197–202, (2014). https://doi.org/10.4028/www.scientific.net/AMR.1077.197.

[49] ASTM E90-09 Standard Test Method for Laboratory Measurement of Airborne Sound Transmission Loss of Building Partitions and Elements, (2016). https://doi.org/10.1520/E0090-09R16.

[50] Bolt, R.H. Note on Normal Frequency Statistics for Rectangular Rooms, *Journal of the Acoustical Society of America*, **18**, 130–133, (1946). https://doi.org/10.1121/1.1916349.

[51] Schroeder, M.R. and Kuttruff, K.H. On Frequency Response Curves in Rooms. Comparison of Experimental, Theoretical, and Monte Carlo Results for the Average Frequency Spacing between Maxima, *The Journal of the Acoustical Society of America*. (1962). https://doi.org/10.1121/1.1909022.

[52] Dammak, K., El Hami, A., Koubaa, S., Walha, L. and Haddar, M. Reliability based design optimization of coupled acoustic-structure system using generalized polynomial chaos, *International Journal of Mechanical Sciences*, **134**, 75–84, (2017). https://doi.org/10.1016/j.ijmecsci.2017.10.003.

[53] Blatman, G. and Sudret, B. Sparse polynomial chaos expansions and adaptive stochastic finite elements using a regression approach, *Comptes Rendus - Mecanique*, **336**, 518–523, (2008). https://doi.org/10.1016/j.crme.2008.02.013.

[54] Dammak, K., Koubaa, S., Elhami, A., Walha, L. and Haddar, M. Numerical modeling of uncertainty in acoustic propagation via generalized polynomial chaos, *Journal of Theoretical and Applied Mechanics* (Poland), **57**, 3–15, (2019). https://doi.org/10.15632/jtam-pl.57.1.3.

[55] ASTM C423-17 Standard Test Method for Sound Absorption and Sound Absorption Coefficients by the Reverberation Room Method, (2017). https://doi.org/10.1520/C0423-17.

[56] Norton, M.P. and Karczub, D.G. Fundamentals of Noise and Vibration Analysis for Engineers, 2nd ed., Cambridge University Press, Cambridge, (2007).

[57] Nélisse, H. and Nicolas, J. Characterization of a diffuse field in a reverberant room, *The Journal of the Acoustical Society of America*, **101**, 3517–3524, (1997). https://doi.org/10.1121/1.418313.